Dielectric Properties of Thermally Aged Polypropylene Nanocomposites

A. Azmi, K. Y. Lau, *Senior Member, IEEE*, N. A. Ahmad, Z. Abdul-Malek, *Senior Member, IEEE*, C. W. Tan, *Senior Member, IEEE*, K. Y. Ching, and A. S. Vaughan

***Abstract*— This article reports on an investigation into the effects of thermal aging on the structure and dielectric properties of polypropylene (PP) nanocomposites. Magnesium aluminate ($MgAl_2O_4$), calcium carbonate ($CaCO_3$), and surface-modified calcium carbonate ($CaCO_3T$) nanofillers have been added to PP and the resulting nanocomposites have been subjected to aging at 110 °C and 140 °C. The results show that unfilled PP experiences a 13% reduction in its dc breakdown strength after aging at 110 °C and that its dc breakdown strength reduces by 27% after aging at 140 °C. In contrast, the reduction in the dc breakdown strength of all investigated PP nanocomposites is much less pronounced than that of the unfilled PP after aging. Specifically, the dc breakdown strength of PP/$MgAl_2O_4$ nanocomposites, PP/$CaCO_3$ nanocomposites, and PP/$CaCO_3T$ nanocomposites reduces by 8%, 14%, and 14%, respectively, after aging at 140 °C. Possible mechanisms affecting the dc breakdown strength of the unfilled PP and PP nanocomposites before and after aging are consequently discussed.**

***Index Terms*— Aging, calcium carbonate, dielectric breakdown, magnesium aluminate, nanocomposites, polypropylene.**

I. Introduction

THE dielectric properties of polymeric insulation deteriorate as a result of various environmental stresses. Specifically, exposure to heat is a main contributor that gives rise to degradation in polymeric insulation. To date, various studies of the aging of cross-linked polyethylene (XLPE) have been carried out and findings on the effects of aging on XLPE have been well documented. For instance, Kim *et al.* [1] reported that thermo-oxidative aging of XLPE at 120 °C resulted in the presence of carbonyl groups. In addition, the melting peak of aged XLPE was modified, suggesting that thermal aging promoted chain scission and oxidation reactions, which reduced the ac resistivity. Meanwhile, Dalal *et al.* [2] attempted to identify and quantify the degradation of XLPE cables based on carbon/hydrogen stretching vibration using the Fourier transform infrared (FTIR) analysis and established accelerated laboratory aging procedures for XLPE where a strong correlation between electric field and sample aging effects could be observed using the well-known Arrhenius equation. Ouyang *et al.* [3] reported that thermo-oxidative aging of XLPE at 100 °C (i.e., below the polymer's peak melting temperature) resulted in oxidative degradation of the amorphous regions, but not the crystalline regions, as a result of oxygen being excluded from the latter phase due to its increased density. However, by aging XLPE at 160 °C (i.e., above the polymer's peak melting temperature), thermo-oxidative aging affected both the amorphous regions and the crystalline structure that subsequently formed on cooling. Kemari *et al.* [4] found that aging XLPE at higher temperatures within the melt phase (120 °C and 140 °C) introduced more polar moieties, which both impeded recrystallization and increased the dielectric constant. Nedjar [5] also reported that the electrical properties of XLPE used in power cables were affected by thermal aging and that the degradation of XLPE became more pronounced with increasing aging temperatures. Specifically, the degradation of XLPE from thermo-oxidation caused color changes in the material with increased dielectric losses and decreased volume resistivity. In summary, the aging behavior of XLPE has been widely studied and such work has shown that the consequences depend on whether aging is conducted above or below the polymer's melting temperature.

In view of the drawbacks of XLPE with regard to the practical operation of cables at elevated temperatures, alternative insulation materials have been explored. Notably, polypropylene (PP)-based materials have attracted significant research attention in the dielectrics community due to the materials having higher melting temperatures compared to XLPE. Specifically, the melting temperature of PP can reach ∼165 °C, compared to ∼105 °C of XLPE [6]. This translates into a higher temperature operating limit for PP compared to XLPE. In addition, PP can be recycled with ease due to its thermoplastic nature. The absence of the crosslinking process in preparing PP-based materials also simplifies manufacturing, where the removal of crosslinking by-products, as required for XLPE-based insulation, is no longer required.

Manuscript received August 24, 2021; accepted March 7, 2022. Date of publication March 31, 2022; date of current version May 2, 2022. This work was supported in part by the Malaysia Ministry of Higher Education and Universiti Teknologi Malaysia (UTM), in part by the Fundamental Research Grant Scheme (FRGS) under Grant FRGS/1/2019/TK04/UTM/02/1 (5F158), in part by Research University Grants under Grant 02M54 and Grant 16J55, and in part by the UTM Zamalah Scholarship. *(Corresponding author: K. Y. Lau.)*

A. Azmi, K. Y. Lau, N. A. Ahmad, Z. Abdul-Malek, and C. W. Tan are with the School of Electrical Engineering, Universiti Teknologi Malaysia, Johor Bahru 81310, Malaysia (e-mail: kwanyiew@utm.my).

K. Y. Ching is with the Foundation, Study and Language Institute, University of Reading Malaysia, Iskandar Puteri 79200, Malaysia.

A. S. Vaughan is with the Department of Electronics and Computer Science, University of Southampton, Southampton SO17 1BJ, U.K.

Color versions of one or more figures in this article are available at https://doi.org/10.1109/TDEI.2022.3163796.

Digital Object Identifier 10.1109/TDEI.2022.3163796

In line with the development of PP-based insulation materials, PP-based nanocomposites have also received attention for dielectric applications, including capacitors and insulators. This is mainly due to the desirable breakdown strength and permittivity of PP nanocomposites while maintaining acceptable dielectric losses [7]–[9]. In contrast to unfilled PP, the incorporation of nanofillers into PP reduces the magnitude of space charge in PP and this effect is more apparent at higher nanofiller loading levels [10]. This shows that nanofillers can suppress charge injection in PP nanocomposites [11], [12]. The use of nanofillers in PP can also improve the dc volume resistivity of the resulting nanocomposites [13].

Recently, we have considered the effects of different multi-element oxide nanofillers on the structure and dielectric properties of PP nanocomposites and emphasized the importance of engineering local interactions between nanoparticles and the surrounding polymer to achieve the desirable dielectric properties [14]. As far as we are aware, the available literature on aging of PP and its nanocomposites is scarce. Therefore, the work reported here sets out to extend our previous study by considering the effects of different aging temperatures, i.e., 110 °C and 140 °C, on the structure and dielectric properties of unfilled PP and PP nanocomposites containing magnesium aluminate ($MgAl_2O_4$), calcium carbonate ($CaCO_3$), and surface-modified calcium carbonate ($CaCO_3T$) nanofillers. These aging temperatures were specifically chosen to be below the peak melting temperature of PP such that aging was conducted in the solid state and, therefore, under conditions relevant to practical cable insulation.

II. Experiment

A. Materials and Blending

In this research, a PP blend composed of 50 wt% of a PP homopolymer (isotactic, grade TITANPRO 6531M) and 50 wt% of a PP impact copolymer (grade TITANPRO SM340), obtained from Lotte Chemical Titan, was used as the polymer matrix. Meanwhile, $MgAl_2O_4$, $CaCO_3$, and $CaCO_3T$ with a manufacturer-quoted particle size of less than 50 nm were used as nanofillers. $MgAl_2O_4$ was obtained from Sigma Aldrich, while $CaCO_3$ and $CaCO_3T$ were obtained from SkySpring Nanomaterials. The nanofiller loading levels were 1 wt%, 2 wt%, and 5 wt%.

A Brabender melt mixer was used to prepare unfilled PP and PP nanocomposites containing $MgAl_2O_4$, $CaCO_3$, and $CaCO_3T$ nanofillers. The rotational speed, temperature, and duration of the mixer were set at 50 r/min, 180 °C, and 10 min, respectively. After melt mixing, samples 100 μm in thickness were produced using a hydraulic laboratory press set at 180 °C and a load of 3 T. The melt-pressed samples were left to cool down naturally under ambient laboratory conditions, before being subjected to thermal aging under vacuum at two different temperatures, namely, 110 °C and 140 °C, for 360 h; unaged samples were also used for comparative assessment purposes. For convenience, all prepared samples are denoted using the general notation "P/F/A," where P refers to the polymer, F signifies the nanofiller and amount, and A represents the aging conditions. For example, PP/0/0 represents unfilled PP not subjected to aging, while PP/$CaCO_3$-2/140 represents PP nanocomposites containing 2 wt% of $CaCO_3$ aged at 140 °C.

B. Characterization

Thermogravimetric analysis (TGA) was carried out using a Perkin Elmer TGA 4000 instrument to examine mass changes as a function of temperature. This measurement was conducted under a nitrogen atmosphere from 30 °C to 900 °C at a scan rate of 10 °C min^{-1}. For each measurement, 5 mg of sample was used.

To investigate further the thermal behavior of the materials, differential scanning calorimetry (DSC) was performed using a Perkin Elmer DSC6. For each measurement, 5 mg of the required sample was prepared and sealed in an aluminum pan. The measurements were conducted under a nitrogen atmosphere. During each DSC scan, the sample was first heated from 60 °C to 180 °C at a scan rate of 10 °C min^{-1}, to characterize its melting behavior. Next, the sample was cooled from 180 °C to 60 °C at a scan rate of 10 °C min^{-1} to determine its crystallization behavior. Perkin Elmer's Pyris software was used to analyze the resulting data. For calibration purposes, high purity indium, with a known melting temperature of 156.6 °C and melting enthalpy of 28.45 J g^{-1}, was used.

Dielectric response measurements were conducted to obtain the dielectric constant, ε_r, of film samples using a Gamry Instruments Interface 1000 with a Tettex 2914 test cell for solid insulation (25-mm radius inner guarded electrode). The measurements were carried out using the low noise optimization setting, by applying a 1-V ac signal over a frequency range of 100 Hz–100 kHz at 20 points per decade.

The dc breakdown tests were conducted using a dielectric strength tester, in accordance with the ASTM D3755 standard. Each sample was placed between two 6.3-mm-diameter steel ball electrodes and, to prevent surface discharges, was immersed in mineral oil during the measurements. A step voltage of 2 kV every 20 s was applied until sample breakdown. Fifteen breakdown points were recorded for each sample type and analyzed using the two-parameter Weibull statistical distribution method.

III. Results

A. Thermogravimetric Analysis

Fig. 1 contains the TGA data obtained from all the systems considered here. For convenience—and to facilitate comparison—we will discuss the degradation process of each in terms of two temperatures that correspond to 5% mass loss ($T_{5\%}$) and 50% mass loss ($T_{50\%}$). Before aging, the unfilled PP was characterized by $T_{5\%} = 337$ °C and $T_{50\%} = 400$ °C; these values fell to 322 °C and 385 °C, respectively, after aging at 110 °C, falling further to 305 °C and 371 °C after aging at 140 °C.

In sharp contrast, all PP nanocomposites demonstrated improved $T_{5\%}$ and $T_{50\%}$ values after being subjected to aging. From Fig. 1(b), unaged PP nanocomposites containing 2 wt% of $MgAl_2O_4$ were characterized by $T_{5\%}$ and $T_{50\%}$ values of 406 °C and 451 °C, respectively. After aging at 110 °C, the

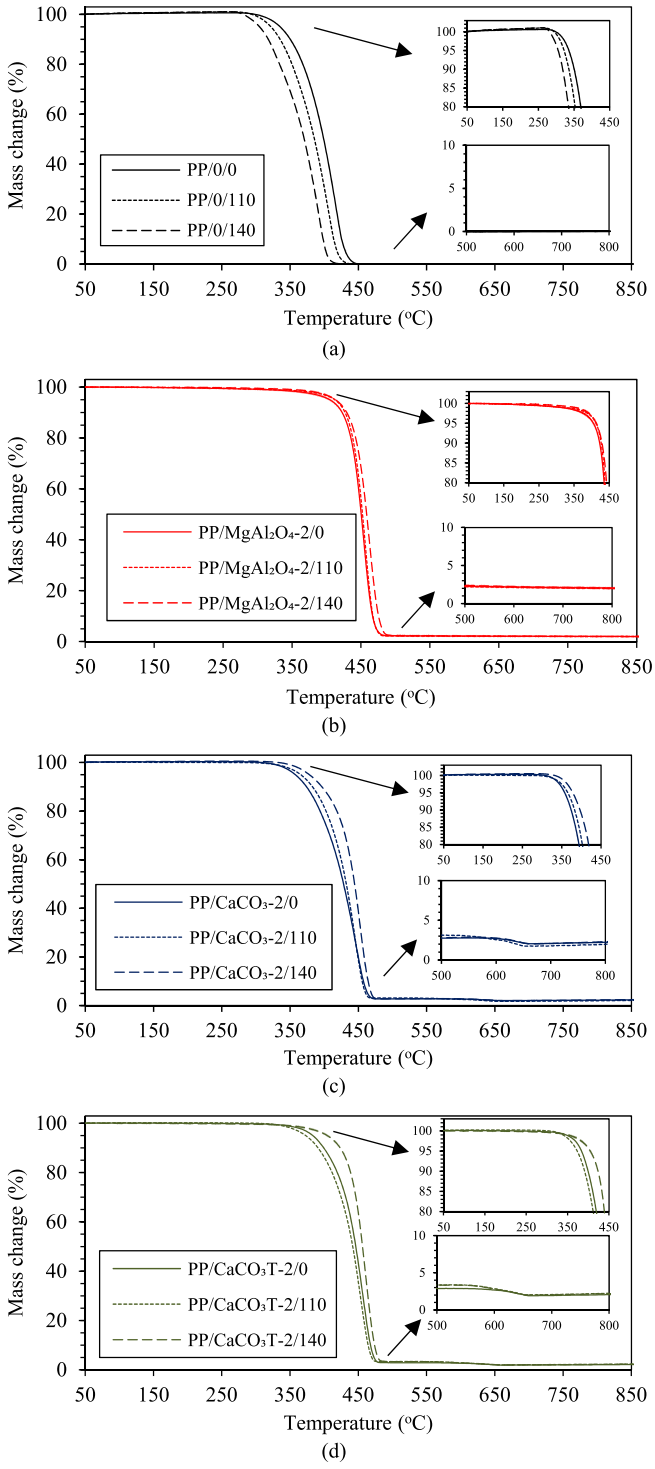

Fig. 1. TGA curve of (a) unfilled PP and PP nanocomposites containing 2 wt% of (b) $MgAl_2O_4$, (c) $CaCO_3$, and (d) $CaCO_3T$ comparing unaged and aged under vacuum condition.

same system gave $T_{5\%} = 412$ °C and $T_{50\%} = 452$ °C, while aging at 140 °C led to slight further increases with $T_{5\%} = 413$ °C and $T_{50\%} = 458$ °C. Similarly, for PP nanocomposites containing 2 wt% of $CaCO_3$ [see Fig. 1(c)] and $CaCO_3T$ [see Fig. 1(d)], $T_{5\%}$ and $T_{50\%}$ generally increased after aging, albeit that aging PP/$CaCO_3T$ nanocomposites at 110 °C slightly reduced $T_{5\%}$ and $T_{50\%}$. Of note, the additional stage of thermal

TABLE I
THERMAL PROPERTIES OF UNFILLED PP AND PP NANOCOMPOSITES AGED AT A DIFFERENT AGING TEMPERATURE

Sample	T_m (°C)	T_c (°C)	Crystallinity (%)
PP/0/0	162	118	46.7
PP/0/110	163	118	47.6
PP/0/140	164	118	53.6
PP/$MgAl_2O_4$-5/0	162	121	54.5
PP/$MgAl_2O_4$-5/110	163	121	55.2
PP/$MgAl_2O_4$-5/140	164	121	60.2
PP/$CaCO_3$-5/0	162	119	51.8
PP/$CaCO_3$-5/110	163	119	55.9
PP/$CaCO_3$-5/140	164	119	58.1
PP/$CaCO_3T$-5/0	162	119	53.2
PP/$CaCO_3T$-5/110	163	119	54.3
PP/$CaCO_3T$-5/140	164	119	59.8

decomposition at ~600 °C shown by the PP/$CaCO_3$ and PP/$CaCO_3T$ nanocomposites is a consequence of the thermal decomposition of the $CaCO_3$ and $CaCO_3T$ nanofillers [14].

A similar trend of improved thermal stability after aging was observed for PP nanocomposites containing 1 wt% and 5 wt% of $MgAl_2O_4$, $CaCO_3$, and $CaCO_3T$, but the respective TGA curves are not shown here for brevity. Rather, the derived $T_{5\%}$ and $T_{50\%}$ values obtained from the unfilled PP and the PP nanocomposites containing 1 wt%, 2 wt%, and 5 wt% of $MgAl_2O_4$, $CaCO_3$, and $CaCO_3T$ before and after aging are succinctly presented in Fig. 2. These data clearly demonstrate the marked improvement in the thermal stability of PP after aging that the presence of the nanoparticles brings.

B. Differential Scanning Calorimetry

Representative DSC thermograms comparing unfilled PP and PP nanocomposites containing $MgAl_2O_4$, $CaCO_3$, and $CaCO_3T$, before and after aging, are shown in Fig. 3; the derived parameters are tabulated in Table I. For brevity, only DSC thermograms for unfilled PP and PP nanocomposites containing 5 wt% of each nanofiller are shown since similar melting traces were obtained from PP nanocomposites containing 1 wt% and 2 wt% of each nanofiller.

From Fig. 3(a), the peak melting temperature of all unaged samples is approximately 162 °C, which corresponds to the fusion of the α-crystal form of PP [8]. The comparable nature of all these DSC melting traces indicates that the addition of $MgAl_2O_4$, $CaCO_3$, or $CaCO_3T$ to PP does not markedly affect the range of lamellar thicknesses present in each material. Of note, a secondary melting peak at 148 °C is indicative of the presence of β-crystals [13]. After aging at 110 °C, the peak melting temperature of all the investigated samples increased slightly to 163 °C and increasing further to 164 °C after aging at 140 °C. This is commensurate with aging occurring within the solid state, leading to annealing of the system and, as shown in Table I, an increase in the measured crystallinity.

DSC cooling traces comparing unaged and aged, unfilled PP, and PP nanocomposites containing $MgAl_2O_4$, $CaCO_3$, and $CaCO_3T$ are shown in Fig. 3(b). The peak in the crystallization exotherm of all the unfilled PP systems is equivalent and is represented by the vertical dashed line in the figure. Adding $MgAl_2O_4$ displaces the crystallization peak to markedly higher

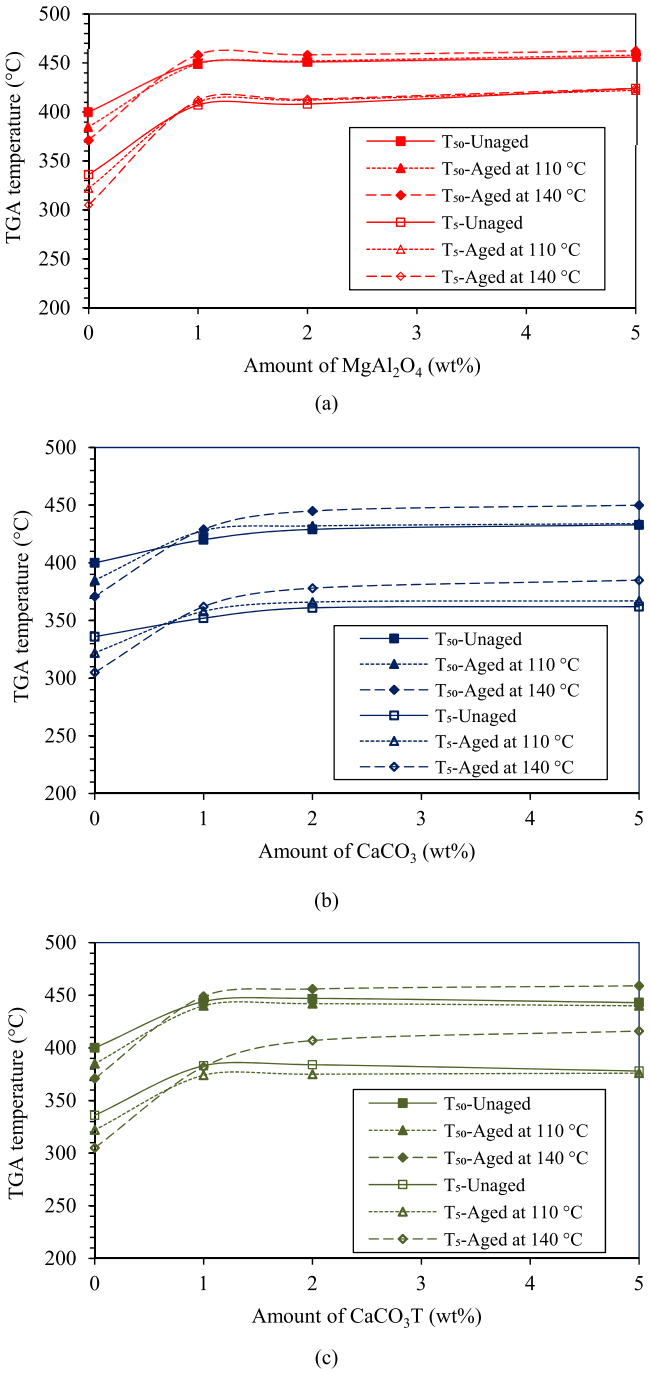

Fig. 2. TGA temperature indicating the thermal stability of unfilled PP and PP nanocomposites containing (a) $MgAl_2O_4$, (b) $CaCO_3$, and (c) $CaCO_3T$ when unaged and aged under vacuum condition.

temperatures and, as previously discussed [14], this is a consequence of the $MgAl_2O_4$ acting as a nucleating agent, whereby its presence modifies the gross matrix morphology of the material and, specifically, the spatial distribution of the different lamellar crystals present in the system. From Table I, it is evident that the crystallization behavior of the systems containing $CaCO_3$, and $CaCO_3T$ is intermediate between that of the unfilled PP and the nanocomposites containing $MgAl_2O_4$, suggesting that it is acting as a mild nucleating agent. This assertion that the addition of all three nanoparticles acts to promote crystallization is further supported by the

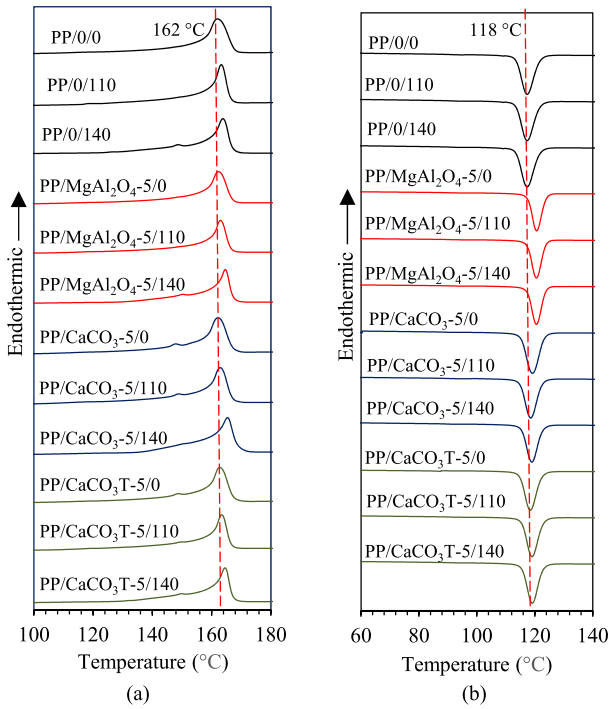

Fig. 3. DSC (a) melting traces and (b) cooling traces comparing unaged and aged and unfilled PP and PP nanocomposites containing $MgAl_2O_4$, $CaCO_3$, and $CaCO_3T$.

crystallinity values obtained from all four unaged PP systems; all unaged nanocomposites exhibit an increase in crystallinity compared with the unaged, unfilled PP. Finally, from Table I, prior aging at 110 °C and 140 °C does not affect the peak crystallization temperature, implying that thermal aging has a negligible effect on the crystallizability of each material and, by implication, has not affected the range of molecular architectures present in the PP matrix.

C. DC Breakdown

Table II summarizes the dc breakdown parameters obtained from both the unaged and aged systems. Aging unfilled PP at either 110 °C or 140 °C led to a significant decrease in the dc breakdown strength of the material. Before aging, unfilled PP was characterized by a dc breakdown strength of 323 ± 18 kV mm^{-1}, which was reduced by 13% and 27% after aging at 110 °C and 140 °C, respectively. In contrast, it is evident from Table II that the effect of aging on the dc breakdown strength of all the PP/$MgAl_2O_4$ nanocomposites was less pronounced, with reductions of just 2%–5% and 3%–8% evident after aging at 110 °C and 140 °C, respectively. For PP nanocomposites containing $CaCO_3$, aging the materials at 110 °C led to a reduction in dc breakdown strength of 7%–10%, while aging at 140 °C reduces this by 13%–20%. Finally, the effect of aging on the dc breakdown behavior of the PP/$CaCO_3T$ nanocomposites was equivalent to that of the nanocomposites containing $CaCO_3$, with comparable fractional reductions being seen on aging at both 110 °C and 140 °C.

The above effects are represented graphically in Fig. 4, in which dc breakdown data obtained from all the investigated samples are normalized with respect to the breakdown strength

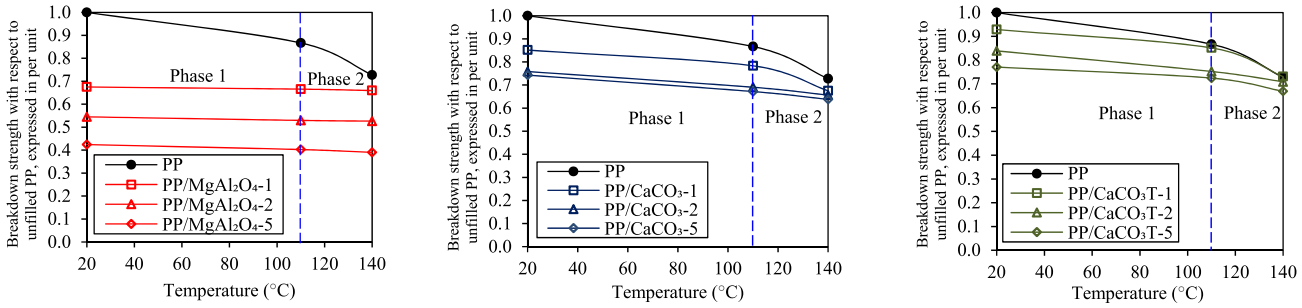

Fig. 4. DC breakdown reduction (expressed in per unit) of unfilled PP with PP nanocomposites containing (a) $MgAl_2O_4$, (b) $CaCO_3$, and (c) $CaCO_3T$ with respect to the dc breakdown strength of unaged and unfilled PP.

TABLE II
DC BREAKDOWN PARAMETERS

Samples	α_{DC} (kV mm^{-1})	β_{DC}
PP/0/0	323 ± 18	17 ± 8
PP/0/110	280 ± 7	18±6
PP/0/140	235 ± 13	8 ± 3
PP/$MgAl_2O_4$-1/0	218 ± 10	10 ± 4
PP/$MgAl_2O_4$-1/110	215 ± 10	10 ± 3
PP/$MgAl_2O_4$-1/140	213 ± 10	8 ± 3
PP/$MgAl_2O_4$-2/0	176 ± 6	13 ± 5
PP/$MgAl_2O_4$-2/110	171 ±10	8 ± 2
PP/$MgAl_2O_4$-2/140	170 ± 6	11 ± 5
PP/$MgAl_2O_4$-5/0	137 ± 10	7 ± 3
PP/$MgAl_2O_4$-5/110	130 ± 7	8 ± 2
PP/$MgAl_2O_4$-5/140	126 ± 11	6 ± 1
PP/$CaCO_3$-1/0	275 ± 11	11±4
PP/$CaCO_3$-1/110	253 ± 6	20 ± 7
PP/$CaCO_3$-1/140	218 ± 6	16 ± 7
PP/$CaCO_3$-2/0	245 ± 12	9 ± 3
PP/$CaCO_3$-2/110	223 ± 6	16 ± 6
PP/$CaCO_3$-2/140	212 ± 7	15 ± 6
PP/$CaCO_3$-5/0	240 ± 6	14 ± 5
PP/$CaCO_3$-5/110	217 ± 9	10 ± 4
PP/$CaCO_3$-5/140	206 ± 7	14 ± 5
PP/$CaCO_3$T-1/0	300 ± 7	20 ± 7
PP/$CaCO_3$T-1/110	275 ± 6	20 ± 8
PP/$CaCO_3$T-1/140	236 ± 9	13 ± 5
PP/$CaCO_3$T-2/0	271 ± 19	7 ± 2
PP/$CaCO_3$T-2/110	243 ± 11	10 ± 4
PP/$CaCO_3$T-2/140	229 ± 10	10 ± 5
PP/$CaCO_3$T-5/0	249 ± 8	14 ± 6
PP/$CaCO_3$T-5/110	234 ± 8	12 ± 4
PP/$CaCO_3$T-5/140	216 ± 11	9 ± 3

TABLE III
PARAMETERS REPRESENTING THE DC BREAKDOWN REDUCTIONS AFTER AGING

Samples	n_1	n_2
PP	0.15	0.47
PP/$MgAl_2O_4$-1	0.01	0.02
PP/$MgAl_2O_4$-2	0.02	0.01
PP/$MgAl_2O_4$-5	0.02	0.04
PP/$CaCO_3$-1	0.08	0.36
PP/$CaCO_3$-2	0.08	0.11
PP/$CaCO_3$-5	0.08	0.11
PP/$CaCO_3$T-1	0.09	0.40
PP/$CaCO_3$T-2	0.10	0.14
PP/$CaCO_3$T-5	0.05	0.19

of the reference, unfilled, and unaged PP. Phase 1 represents the possible variation in the dc breakdown strength of the samples below the aging temperature of 110 °C (the unaged temperature is estimated at room temperature of 20 °C), while phase 2 represents the variation in dc breakdown strength of aged samples over the temperature range 110 °C–140 °C. The rate of variation in the normalized breakdown strength with aging temperature, n_1 and n_2 of the plots in Fig. 4 under phases 1 and 2, respectively, is summarized in Table III. Higher n_1 and n_2 values translate into greater reductions in dc breakdown strength with respect to unaged PP.

From Table III, the per-unit reduction in the dc breakdown strength of the unfilled PP is more significant than for the PP nanocomposites, where n_1 for unfilled PP was 0.15. A further reduction in the dc breakdown strength of unfilled PP can be observed in phase 2, where n_2 increased markedly to 0.47. This indicates that the unfilled PP suffered from much reduced dc breakdown strength after aging at higher temperatures. Although the dc breakdown strength of PP nanocomposites fell after aging, the effects were less pronounced compared to unfilled PP. For example, PP nanocomposites containing 5 wt% of $MgAl_2O_4$ had n_1 and n_2 values of just 0.02 and 0.04, respectively. These values are significantly lower than those of the unfilled PP. As in the case of the PP/$MgAl_2O_4$ systems, the PP/$CaCO_3$ and PP/$CaCO_3$T nanocomposites are also characterized by lower n_1 and n_2 values than the unfilled PP; the n_1 and n_2 values of the PP/$CaCO_3$ and PP/$CaCO_3$T nanocomposites are, however, generally higher than those of the PP/$MgAl_2O_4$ nanocomposites.

D. Dielectric Response

Fig. 5 shows the frequency dependence of the real part of the relative permittivity, ε', of unfilled PP and representative PP nanocomposite samples containing $MgAl_2O_4$, $CaCO_3$, and $CaCO_3T$ before and after aging. For ease of comparison, Fig. 6 presents ε' at 10 kHz for the unfilled PP and all the investigated nanocomposites before and after aging. Of note, the unfilled PP shows a noticeable increase in ε' after aging; for this system, $\varepsilon' = 2.69$ before aging, while, after aging this increased to, 2.78 in the case of sample aged at 110 °C and 2.93 when aged at 140 °C. Comparable aging effects have been reported elsewhere [5], [14], [15]. Although ε' of the unfilled PP before aging is slightly higher than that of the theoretical value (about 2.2), it is not peculiar to obtain slightly higher ε' of PP, as has been reported elsewhere in the literature [16]–[18].

While unfilled PP exhibited an significant increase in ε' after aging, the observed increases were much less for PP/$MgAl_2O_4$

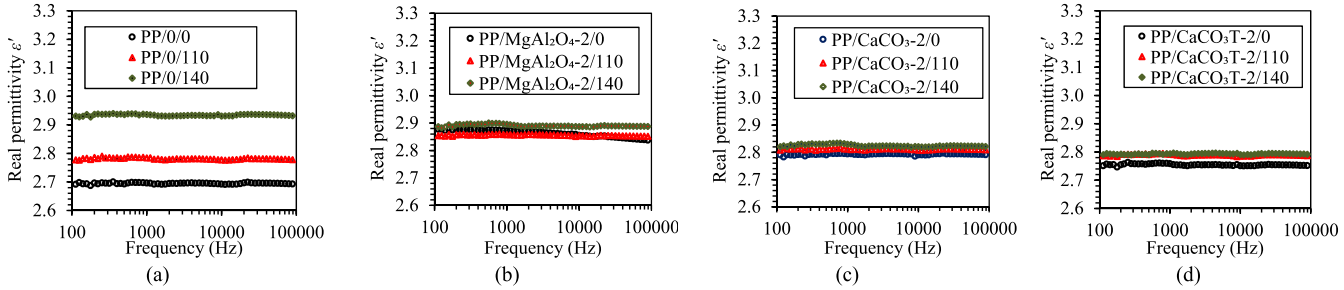

Fig. 5. Real permittivity of unfilled PP and PP nanocomposites containing 2 wt% of (a) $MgAl_2O_3$, (b) $CaCO_3$, and (d) $CaCO_3T$ of unaged and aged.

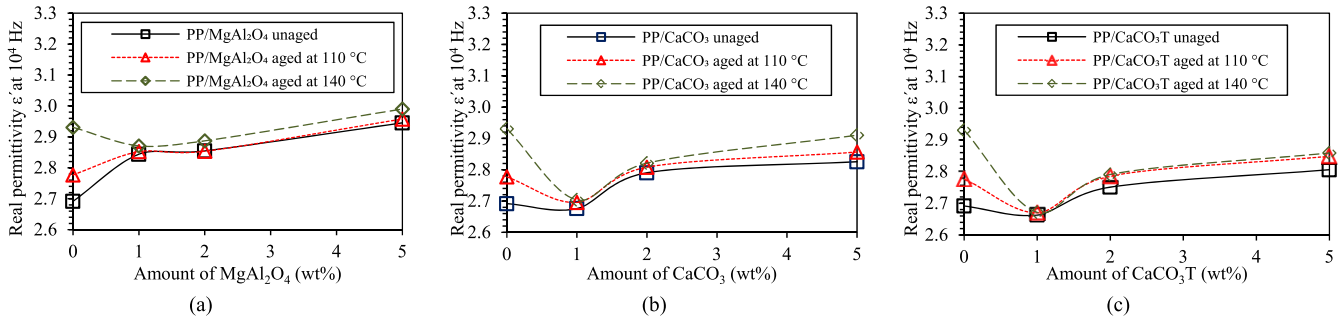

Fig. 6. Real permittivity at 10 kHz for unfilled PP and nanocomposites containing (a) $MgAl_2O_3$, (b) $CaCO_3$, and (c) $CaCO_3T$ at different aging temperatures.

nanocomposites. For example, at 10 kHz, the real part of the relative permittivity of unaged PP nanocomposites containing 2 wt% of $MgAl_2O_4$ was 2.85, remaining unchanged after aging at 110 °C and increasing only marginally to 2.89 after aging at 140 °C. Aging at 110 °C and 140 °C also led to a marginal increase in the real permittivity of PP/$CaCO_3$ nanocomposites. For example, in the case of the unaged PP nanocomposites containing 2 wt% of $CaCO_3$, $\varepsilon' = 2.79$ at 10 kHz; after aging at 110 °C, this increased to 2.81 and after aging at 140 °C to 2.82. A similar trend of marginal increases in the real permittivity value was observed for PP/$CaCO_3T$ nanocomposites after aging at 110 °C and 140 °C. Therefore, all the PP nanocomposites demonstrated only a slight increase in the real relative permittivity after aging.

In our previous work [14], ε' of nanocomposites containing 1 wt% of $CaCO_3$ and $CaCO_3T$ before aging can be lower than that of the unfilled PP. Here, similar observations are found after aging. This reinforces our previous assertion that the reduced ε' seen in the nanocomposite systems is a consequence of local, interfacial effects that occur in the materials. The increase of ε' of the nanocomposites with increasing nanofiller content is in line with some observations reported in the literature [13], [19] and hence not discussed further. Of note, the imaginary permittivity, ε'', values of all the samples is very low, at the limit of the sensitivity of the measurement equipment; and these data are therefore not shown, as has been reported in our previous studies [14], [20].

IV. Discussion

The results presented above reveal that aging of the unfilled PP and all associated nanocomposite systems results in changes in a number of physical properties and that these are strongly formulation-dependent. First, we have shown that while the TGA thermal stability of unfilled PP is reduced after aging, and an increase in the TGA thermal stability of all the investigated nanocomposites occurs. Second, while the dc breakdown strength of all the investigated materials was reduced as a consequence of aging, the unfilled PP was characterized by a much greater fractional reduction than any of the nanocomposite systems. Finally, while the real part of the relative permittivity of the materials generally increased after aging, this was much more pronounced in the case of the unfilled PP than in the nanocomposites. In short, the influence of aging was, in all three of these respects, much more pronounced in the unfilled PP than in the equivalent nanocomposites. In this regard, the nanocomposites appear more aging-resistant.

To explain the above effects, it is necessary to consider how the chosen aging protocol can affect each system and such changes can broadly be classified as either chemical or physical. Considering chemical changes first, it is of note that the FTIR spectra of all samples were acquired but are not shown for the sake of brevity, as they reveal no significant changes in the chemical compositions of the materials after aging [14]. This is attributed to aging being conducted in vacuum, whereby oxidation would be precluded [21]–[23]. Consequently, we suggest that the primary effect of the aging protocol used here is to change the structure of each system and, indeed, the DSC data presented provide a number of key indicators of the physical aging effects that occur in each system. Specifically, it is evident that the aging imposed here results in a minor increase in peak melting temperature together with a pronounced increase in the crystallinity of each system. Since the peak melting temperature measured by DSC can be influenced by structural reorganization during the course of the DSC scan, small changes in this parameter should be handled with care. Conversely, the marked increases in crystallinity seen in all aged samples provide clear evidence that holding such systems at elevated temperatures for a prolonged period induces structural reorganization, as also

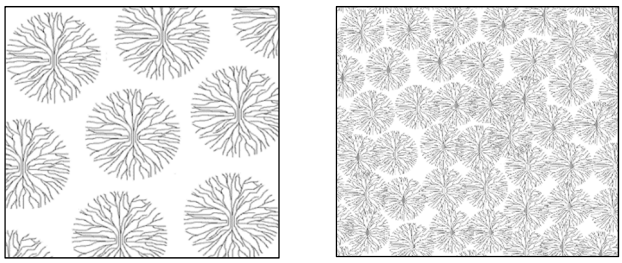

Fig. 7. Illustration of (a) large spherulites within unfilled PP and (b) small spherulites within PP/$MgAl_2O_4$ nanocomposites, separated by the amorphous phase.

reported elsewhere [24], [25]. It is important, here, to recognize that these aging temperatures were deliberately chosen to be below the peak melting temperature of all of these systems and that, therefore, these structural changes are occurring within the lamellar framework of these semicrystalline systems. Consider, first, the unfilled PP.

Slowly crystallized PP, as produced here, is generally characterized by a morphology based on large spherulites. This is shown in Fig. 7(a). While annealing such structure will result in increased crystallinity, as shown above, it will not change the spherulitic skeleton of the material, this being based on the most thermodynamically stable dominant lamellae. As such, increasing crystallinity under, effectively, isochoric conditions will, necessarily, result in structural changes within the amorphous phase that equate to a reduction in the amorphous density and an increase in free volume, particularly in those structural regions that contain an excess of segregated, defective molecular forms: the interspherulitic regions. Such a change would be expected to result in a reduction in local molecular constraints, which is consistent with the observed increase in the real part of the relative permittivity of this material after aging. Extending this further, Cubero and Quirke [26], Wang *et al.* [27], and Saiz *et al.* [28] studied in detail charge transport through amorphous regions in polyethylene and concluded that this is strongly associated with local variations in chain packing. In particular, excess electrons propagate via the lowest density regions. As such, the proposal that aging results in increased amorphous free volume would be expected to enhance electron mobility, which explains the observed reduction in dc breakdown strength seen on aging. In many ways, this has parallels with previous proposals concerning the mechanisms by which thermo-oxidative aging results in reduced breakdown strength, albeit that postoxidation, charge transport is envisaged as being mediated by chemical defects, whereas, here, we see this as resulting from structural changes in the amorphous phase. A similar observation was found in the research conducted by Ieda [29], where an increase in the crystallinity level of the polymer when aged under elevated temperature led to a reduction in their dc breakdown strength.

Now, consider the behavior of the nanocomposite systems, which, on grounds of brevity, we will consider collectively. From the DSC cooling data, we deduce that all three nanoparticles act to nucleate the PP; systems containing $MgAl_2O_4$ exhibit greater elevations in the temperature of the crystallization exotherm than those containing $CaCO_3$ and $CaCO_3T$, implying that $MgAl_2O_4$ is a more effective nucleant than $CaCO_3$ and $CaCO_3T$ [30]–[32]. The implications of this are: 1) systems containing $MgAl_2O_4$ will contain smaller spherulites than systems containing $CaCO_3$ and $CaCO_3T$ and 2) the interspherulitic regions will be less well defined in systems containing $MgAl_2O_4$ than in systems containing $CaCO_3$ and $CaCO_3T$ [see the illustration in Fig. 7(b)]. Extending the interpretation proposed above, whereby changes in the local amorphous structure in interspherulitic regions are the root cause of the aging-induced increase in ε_r' and the decrease in dc breakdown strength seen in the unfilled PP then, from this, we would infer that the aging should have a lesser effect in $CaCO_3$- and $CaCO_3T$-based nanocomposites and the least effect in systems containing $MgAl_2O_4$. This is exactly what is seen experimentally. In other words, the effect of structural changes within the amorphous phase that equate to an increase in free volume becomes limited in the nanocomposite systems, especially those containing $MgAl_2O_4$. Consequently, a limited change would be expected in local molecular constraints, which is consistent with the limited increase in the real part of the relative permittivity of the nanocomposite systems after aging. Furthermore, this assertion that the local structure of interspherulitic regions plays a critical role in breakdown precisely aligns with the work of Kolesov [33] and Hosier *et al.* [34].

Finally, consider the TGA behavior and, specifically, the contrary trends seen in the unfilled PP and the PP-based nanocomposites. The rate of mass loss within a TGA experiment is determined by two factors: the rate of production of volatile molecular fractions and their rate of diffusion out of the sample. In the case of nanocomposites, the commonly reported improvement in thermal stability or reduced flammability is conventionally explained in terms of enhanced char generation through the catalytic activity of impurities within the nanoparticles, which serves: 1) to prevent migration of volatile decomposition products out of the decomposing solid (the fuel, in the case of flammability) and 2) to prevent diffusion of oxygen into the system that leads to chain scission and, hence, the rate of production of volatiles. This association of permeability with decomposition therefore, again, aligns well with the proposal made above that the origin of the changes in electrical properties seen in the various systems is related to: 1) changes in free volume in amorphous regions; 2) the local nature of these is strongly influenced by the morphology of each system; and 3) the nucleation density is critical in defining this. While this provides an explanation for the marked difference in behavior between the unfilled PP (no nucleating agent hence large spherulites) and the nanocomposites (nucleating agents hence small spherulites), understanding of the more subtle differences in behavior between the various nanocomposites requires a more detailed study of their decomposition kinetics.

V. Conclusion

In the current work, we report on the effects of aging on the structure and dielectric properties of unfilled PP, PP/$MgAl_2O_4$

nanocomposites, PP/$CaCO_3$ nanocomposites, and PP/$CaCO_3$T nanocomposites. Notably, aging of unfilled PP and all associated nanocomposite systems results in changes in a number of physical properties that are formulation-dependent: 1) the TGA thermal stability of unfilled PP reduces after aging, but an increase in the TGA thermal stability of all the investigated nanocomposites occurs; 2) the dc breakdown strength of all the investigated materials reduces as a consequence of aging temperature, with the unfilled PP characterized by a much greater fractional reduction than any of the nanocomposite systems; and 3) the real part of the relative permittivity of the materials generally increases after aging and this is much more pronounced in the case of the unfilled PP than in the nanocomposites. We, therefore, suggest that the primary effect of the aging seen here is to change the structure of each material system. Specifically, aging results in changes in the local amorphous structure in interspherulitic regions that equate to an increase in free volume, which enhances electron mobility, thus increasing the real part of the relative permittivity and reducing the dc breakdown strength of the unfilled PP. Since all the nanocomposites appear more aging-resistant than the unfilled PP, we associate this to smaller spherulites and less well-defined interspherulitic regions within the nanocomposites as a consequence of nanoparticle nucleation.

REFERENCES

[1] C. Kim, Z. Jin, P. Jiang, Z. Zhu, and G. Wang, "Investigation of dielectric behavior of thermally aged XLPE cable in the high-frequency range," *Polym. Test.*, vol. 25, no. 4, pp. 553–561, Jun. 2006.

[2] S. B. Dalal, R. S. Gorur, and M. L. Dyer, "Aging of distribution cables in service and its simulation in the laboratory," *IEEE Trans. Dielectr. Electr. Insul.*, vol. 12, no. 1, pp. 139–146, Feb. 2005.

[3] B. Ouyang, H. Li, X. Zhang, S. Wang, and J. Li, "The role of microstructure changes on space charge distribution of XLPE during thermo-oxidative ageing," *IEEE Trans. Dielectr. Electr. Insul.*, vol. 24, no. 6, pp. 3849–3859, Dec. 2017.

[4] Y. Kemari, A. Mekhaldi, G. Teyssedre, and M. Teguar, "Correlations between structural changes and dielectric behavior of thermally aged XLPE," *IEEE Trans. Dielectr. Electr. Insul.*, vol. 26, no. 6, pp. 1859–1866, Dec. 2019.

[5] M. Nedjar, "Effect of thermal aging on the electrical properties of crosslinked polyethylene," *J. Appl. Polymer Sci.*, vol. 111, no. 4, pp. 1985–1990, Feb. 2009.

[6] Y. Xie, Y. Zhao, G. Liu, J. Huang, and L. Li, "Annealing effects on XLPE insulation of retired high-voltage cable," *IEEE Access*, vol. 7, pp. 104344–104353, 2019.

[7] Y. Wang, X. Zhou, Q. Chen, B. Chu, and Q. Zhang, "Recent development of high energy density polymers for dielectric capacitors," *IEEE Trans. Dielectr. Electr. Insul.*, vol. 17, no. 4, pp. 1036–1042, Aug. 2010.

[8] Y. Zhou *et al.*, "Temperature dependent electrical properties of thermoplastic polypropylene nanocomposites for HVDC cable insulation," *IEEE Trans. Dielectr. Electr. Insul.*, vol. 26, no. 5, pp. 1596–1604, Oct. 2019.

[9] J.-W. Zha, J.-F. Wang, S.-J. Wang, Q. Qin, and Z.-M. Dang, "Effect of modified ZnO on electrical properties of PP/SEBS nanocomposites for HVDC cables," *IEEE Trans. Dielectr. Electr. Insul.*, vol. 25, no. 6, pp. 2358–2365, Dec. 2018.

[10] Z. Li, W. Cao, G. Sheng, X. Jiang, and M. G. Danikas, "Experimental study on space charge and electrical strength of MgO nanoparticles/polypropylene composite," *IEEE Trans. Dielectr. Electr. Insul.*, vol. 23, no. 3, pp. 1812–1819, Jun. 2016.

[11] G. C. Montanari, D. Fabiani, F. Palmieri, D. Kaempfer, R. Thomann, and R. Mulhaupt, "Modification of electrical properties and performance of EVA and, pp. insulation through nanostructure by organophilic silicates," *IEEE Trans. Dielectr. Electr. Insul.*, vol. 11, no. 5, pp. 754–762, Nov. 2004.

[12] B. X. Du, H. Xu, J. Li, and Z. Li, "Space charge behaviors of PP/POE/ZnO nanocomposites for HVDC cables," *IEEE Trans. Dielectr. Electr. Insul.*, vol. 23, no. 5, pp. 3165–3174, Oct. 2016.

[13] Y. Zhou, J. Hu, B. Dang, and J. He, "Effect of different nanoparticles on tuning electrical properties of polypropylene nanocomposites," *IEEE Trans. Dielectr. Electr. Insul.*, vol. 24, no. 3, pp. 1380–1389, Jun. 2017.

[14] A. Azmi *et al.*, "Structure-dielectric property relationship in polypropylene/multi-element oxide nanocomposites," *IEEE Trans. Nanotechnol.*, vol. 20, pp. 377–385, 2021.

[15] M. Nedjar, A. Béroual, and A. Boubakeur, "Influence of thermal aging on the electrical properties of poly(vinyl chloride)," *J. Appl. Polym. Sci.*, vol. 102, no. 5, pp. 4728–4733, Dec. 2006.

[16] D. Xie, D. Min, Y. Huang, S. Li, M. T. Nazir, and B. T. Phung, "Classified effects of nanofillers on DC breakdown and partial discharge resistance of polypropylene/alumina nanocomposites," *IEEE Trans. Dielectr. Electr. Insul.*, vol. 26, no. 3, pp. 698–705, Jun. 2019.

[17] X. Y. Huang, Y. Y. Fan, J. Zhang, and P. K. Jiang, "Polypropylene based thermoplastic polymers for potential recyclable HVDC cable insulation applications," *IEEE Trans. Dielectr. Electr. Insul.*, vol. 24, no. 3, pp. 1446–1456, Jun. 2017.

[18] N. Fuse, Y. Ohki, and T. Tanaka, "Comparison of nano-structuration effects in polypropylene among four typical dielectric properties," *IEEE Trans. Dielectr. Electr. Insul.*, vol. 17, no. 3, pp. 671–677, Jun. 2010.

[19] J. Liu, Y. Wang, K. Xiao, and Z. Zhang, "Research on the thermal aging behaviors of LDPE/TiO2 nanocomposites," *J. Nanomater.*, vol. 2017, p. 11, Jun. 2017.

[20] N. H. Rahim, K. Y. Lau, N. A. Muhamad, N. Mohamad, C. W. Tan, and A. S. Vaughan, "Structure and dielectric properties of polyethylene nanocomposites containing calcined zirconia," *IEEE Trans. Dielectr. Electr. Insul.*, vol. 26, no. 5, pp. 1541–1548, Oct. 2019.

[21] V. A. González-González, G. Neira-Velázquez, and J. L. Angulo-Sánchez, "Polypropylene chain scissions and molecular weight changes in multiple extrusion," *Polym. Degradation Stability*, vol. 60, no. 1, pp. 33–42, Apr. 1998.

[22] E. Esmizadeh, C. Tzoganakis, and T. H. Mekonnen, "Degradation behavior of polypropylene during reprocessing and its biocomposites: Thermal and oxidative degradation kinetics," *Polym. (Basel).*, vol. 12, no. 8, pp. 1–23, Aug. 2020.

[23] J. Aurrekoetxea *et al.*, "Effects of recycling on the microstructure and the mechanical properties of isotactic polypropylene," *J. Mater. Sci.*, vol. 36, pp. 2607–2613, Jun. 2001.

[24] H. Li, J. Li, Y. Ma, Q. Yan, and B. Ouyang, "The role of thermo-oxidative aging at different temperatures on the crystal structure of crosslinked polyethylene," *J. Mater. Sci., Mater. Electron.*, vol. 29, no. 5, pp. 3696–3703, Mar. 2018.

[25] J. R. White, "Polymer ageing: Physics, chemistry or engineering? Time to reflect," *Comp. Rendus Chimie*, vol. 9, nos. 11–12, pp. 1396–1408, Nov. 2006.

[26] D. Cubero and N. Quirke, "Computer simulations of localized small polarons in amorphous polyethylene," *J. Chem. Phys.*, vol. 120, no. 16, pp. 7772–7778, Apr. 2004.

[27] Y. Wang *et al.*, "Single electron states in polyethylene," *J. Chem. Phys.*, vol. 140, no. 15, pp. 154902-1–154902-11, Apr. 2014.

[28] F. Saiz, D. Cubero, and N. Quirke, "The excess electron at polyethylene interfaces," *Phys. Chem. Chem. Phys.*, vol. 20, no. 39, pp. 25186–25194, Oct. 2018.

[29] M. Ieda, "Dielectric breakdown process of polymers," *IEEE Trans. Electr. Insul.*, vol. EI-15, no. 3, pp. 206–224, Jun. 1980.

[30] R. Ayoob, F. Alhabill, T. Andritsch, and A. Vaughan, "Enhanced dielectric properties of polyethylene/hexagonal boron nitride nanocomposites," *J. Mater. Sci.*, vol. 53, no. 5, pp. 3427–3442, Mar. 2018.

[31] I. L. Hosier, M. Praeger, A. S. Vaughan, and S. G. Swingler, "The effects of water on the dielectric properties of silicon-based nanocomposites," *IEEE Trans. Nanotechnol.*, vol. 16, no. 2, pp. 169–179, Mar. 2017.

[32] H. U. Zaman, M. A. Khan, R. A. Khan, and M. D. H. Beg, "Effect of nano-$CaCO_3$ on the mechanical and crystallization behavior of HDPE/LDPE/nano-$CaCO_3$ ternary blend," *J. Thermoplastic Compos. Mater.*, vol. 27, no. 12, pp. 1701–1710, Feb. 2013.

[33] S. N. Kolesov, "The influence of morphology on the electric strength of polymer insulation," *IEEE Trans. Electr. Insul.*, vol. El-15, no. 5, pp. 388–4388, Oct. 1980.

[34] I. L. Hosier, A. S. Vaughan, and S. G. Swingler, "Structure-property relationships in polyethylene blends: The effect of morphology on electrical breakdown strength," *J. Mater. Sci.*, vol. 32, no. 17, pp. 4523–4531, Sep. 1997.